Int. J. Electrochem. Sci., 15 **(2020)** 9233 – 9244, doi: 10.20964/2020.09.27

International Journal of ELECTROCHEMICAL SCIENCE
www.electrochemsci.org

Short Communication

Lithium Plating as Limiting Phenomena for Estimating Safety during Lithium-Ion Battery Charging

Xiaojun Tan[1], *Jianzhi Qiu*[1], *Jun Li*[1,*], *Yuqian Fan*[1], *Jiansheng Liu*[2]

[1] School of Intelligent Systems Engineering, Sun Yat-sen University, Guangzhou, Guangdong Province, 510006, China
[2] Zhuhai Great Power Energy CO., LTD, Zhuhai, Guangdong Province, 519100, China
[*]E-mail: lijun255@mail.sysu.edu.cn (J. Li)

Received: 23 April 2020 / *Accepted:* 4 June 2020 / *Published:* 10 August 2020

During charging, lithium-ion (Li-ion) batteries can undergo lithium plating if the charging current is too high. This process will reduce battery capacity and affect the safety performance of batteries. This paper proposes a method for estimating the allowable maximum charging current for Li-ion batteries at different states of charge (SOCs), employs an electrochemical model, and uses lithium plating as the threshold. The main achievements include (1) developing a new model based on the SP+ model, redescribes some of the equations and parameters used in the SP+ model, and more accurately reflects the conditions of Li-ion battery anodes; (2) determining the specific operating conditions used to identify the model parameters, identifying each model parameter, and performing an error analysis; and (3) using this model to produce relationship diagrams of the anode potential and current versus SOC, thus identifying the allowable maximum charging current for Li-ion batteries at different SOCs.

Keywords: lithium-ion battery, electrochemical model, parameter identification, lithium plating, allowable maximum charging current

1. INTRODUCTION

Lithium-ion (Li-ion) batteries exhibit a high energy density [1]. Li-ion batteries also have advantages such as good electrochemical properties, a high thermal stability, a long life span, a low self-discharge rate, and no memory effects [2,3]. Li-ion batteries are thus increasingly used as power sources for portable electric devices and aerospace applications [4,5]. The research and industrialization of Li-ion batteries have also moved forward rapidly [6]. If the charging current is too high while charging Li-ion batteries, lithium plating can take place, which dramatically reduces the battery capacity [7,8]. The resulting lithium dendrites could pierce the battery separator and cause a short circuit, thus affecting the safety performance of the battery [8]. To avoid lithium plating, a model that can accurately describe the internal conditions of Li-ion batteries needs to be built; such a model can be used to determine the

allowable maximum charging current for Li-ion batteries at different states of charge (SOCs).

The models that have been mainly used in the past include equivalent circuit models (ECMs) and electrochemical models [9,10]. ECMs are composed of electronic components (such as resistance, capacitance, and inductance), whose parameters can be easily obtained by least squares fitting by or intelligent algorithms, such as genetic algorithms (GA) [11,12]. ECMs have the advantages of a high calculational efficiency and highly identifiable parameters, but its absolute estimation errors are higher than those of the electrochemical models[10]. The electrochemical models mainly include pseudo 2-dimensional (P2D) models and their derivatives. [13,14] The P2D model constructed by Newman et al. is a first-principles electrochemical model that accurately describes almost all the physicochemical processes inside Li-ion batteries [15-17]. The P2D model is very versatile and accurate and is currently the most mature electrochemical model. However, the P2D model contains a series of partial differential equations and algebraic equations and has more than 30 parameters that need to be determined, making the calculations very complex during simulations [18]. Thus, the model cannot be used directly for battery management [18]. To simplify the P2D model and increase the calculating efficiency, Atlung and Haran et al. [19,20] proposed an SP model derived from the P2D model. The model assumes that each electrode only consists of one spherical solid particle. The SP model proposed by Atlung and Haran et al. neglects the concentration gradient in the electrolyte, the liquid-phase diffusion overpotential, and the solid-phase concentration distribution along the electrode thickness, thus decreasing the number of partial differential equations and simplifying the calculations. Nevertheless, the simulation error of this SP model at high rates is much larger than that of the P2D model. Luo and Li et al. developed an SP+ model by adding the solid- and liquid-phase ohmic overpotential and concentration overpotential to the SP model [21]. The new model has a relatively high accuracy and is described by ordinary differential equations and algebraic equations, which notably reduces the complexity of calculation [22].

Although the SP+ model has a relatively high simulation accuracy and low calculation complexity, some model parameters are used equally at the cathode and anode, so the anode condition cannot be accurately simulated. To address this issue, this paper redescribes some of the equations and parameters used in the SP+ model. The modified model was used to determine the allowable maximum charging current for batteries at different SOCs. The rest of the paper is organized as follows.

First, some equations and parameters in the SP+ model were redescribed to build the new model in this study. Second, the operating conditions used for parameter identification were set according to the relationship between the model parameters and external battery behaviors, and the precision of the model was validated. Third, the model was used to plot the anode potential and current versus the SOC at 7℃ and 25℃ to determine the allowable maximum charging current for batteries at different SOCs. Finally, conclusions were drawn.

2. EXPERIMENTAL

2.1 Electrochemical model

To identify the relationship between the anode potential and SOC of Li-ion batteries at certain charging rates, the equations and parameters used in the SP+ model were improved, and the model

parameters were divided into cathode parameters and anode parameters, which facilitated the determination of the anode potential.

The following tables list the equations and parameters used in the modified model.

Table 1. Modified model equations

Terminal voltage	$U_{app}(t) = E_{ocv}(t) - \eta_{con}(t) - \eta_{act}(t) - \eta_{ohm}(t)$
Basic process	$E_{ocv}(t) = U_p[y_{surt}(t)] - U_n[x_{surt}(t)]$
	$y_{avg}(t) = y_0 + It/Q_p$
	$x_{avg}(t) = (1 - y_{ofs} - y_{avg})Q_p/Q_n$
	$y_{surt}(t) = y_{avg}(t) + \Delta y(t)$
	$x_{surt}(t) = x_{avg}(t) - \Delta x(t)$
Solid-phase diffusion	$\Delta y(t) = \Delta y'(t) + \frac{2}{7}\frac{\tau_{ps}}{Q_n}I(t)$
	$\Delta x(t) = \Delta x'(t) + \frac{2}{7}\frac{\tau_{ns}}{Q_n}I(t)$
	$\Delta y'(t_{k+1}) = \Delta y'(t_k) + \frac{1}{\tau_n^s}(\frac{12}{7}\frac{\tau_n^s}{Q_n}I(t_k) - \Delta y'(t_k))(t_{k+1} - t_k)$
	$\Delta x'(t_{k+1}) = \Delta x'(t_k) + \frac{1}{\tau_n^s}(\frac{12}{7}\frac{\tau_n^s}{Q_n}I(t_k) - \Delta x'(t_k))(t_{k+1} - t_k)$
Liquid-phase diffusion	$\eta_{con}(t) = \frac{2RT(t)}{F}(1 - t_+)\ln(\frac{c_0 + \Delta c(t)}{c_0 - \Delta c(t)})$
	$\tau_s \Delta c(t_{k+1}) = \Delta c(t_k) + \frac{1}{\tau_e}(p_{con}I(t_k) - \Delta c(t_k))(t_{k+1} - t_k)$
Activation polarization	$\eta_{act}(t) = \frac{2RT(t)}{F}(\ln\left(\sqrt{m_n^2(t)+1} + m_n(t)\right) + \ln\left(\sqrt{m_p^2(t)+1} + m_p(t)\right))$
	$m_p(t) = \frac{1}{6Q_p c_0^{0.5}}\frac{1}{(1 - y_{surt}(t))^{0.5}(y_{surt}(t))^{0.5}}p_{actp}I(t)$
	$m_n(t) = \frac{1}{6Q_n c_0^{0.5}}\frac{1}{(1 - x_{surt}(t))^{0.5}(x_{surt}(t))^{0.5}}p_{actn}I(t)$
Ohmic polarization	$\eta_{ohm}(t) = I(t)R_{ohm}(t)$

Table 2. Model parameters

Parameters	Definitions
y_0	Initial lithium ion concentration at the cathode
x_0	Initial lithium ion concentration at the anode
Δx	Maximum variation in the lithium ion concentration at the cathode
Δy	Maximum variation in the lithium ion concentration at the anode
Q_p	Available capacity of the active materials in the cathode
Q_n	Available capacity of the active materials in the anode
$\boldsymbol{\tau_e}$	Diffusion time constant in the liquid phase
R_{ohm}	Ohmic resistance
$P_{act\,p}$	Polarization coefficient of the cathode reaction
$P_{act\,n}$	Polarization coefficient of the anode reaction
P_{con}	Diffusion ratio coefficient in the liquid phase
τ_{ps}	Solid-phase diffusion time constant at the cathode
τ_{ns}	Solid-phase diffusion time constant at the anode

2.2. Parameter identification

Fig. 1 plots the specific operating conditions used to determine the model parameters. The figure contains three parts.

Part 1: The battery is discharged at 0.1 C for 2 hours to reach an SOC of 0.8 and is then allowed to stand for 30 minutes to recover the concentration polarization. A rest period of 30 minutes is set between each charge and discharge to ensure that the concentration polarization is recovered.

Part 2: The charging currents are 0.25 C, 0.5 C, 1 C, and 2 C, and the discharging currents are 0.5 C, 1 C, 2 C, and 3 C. Constant current charging and discharging are alternately performed at different rates between the battery rest periods, with the former lasting 5 minutes, and the latter lasting 30 minutes.

Part 3: The battery is discharged at a constant current of 0.05 C to reach 3 V.

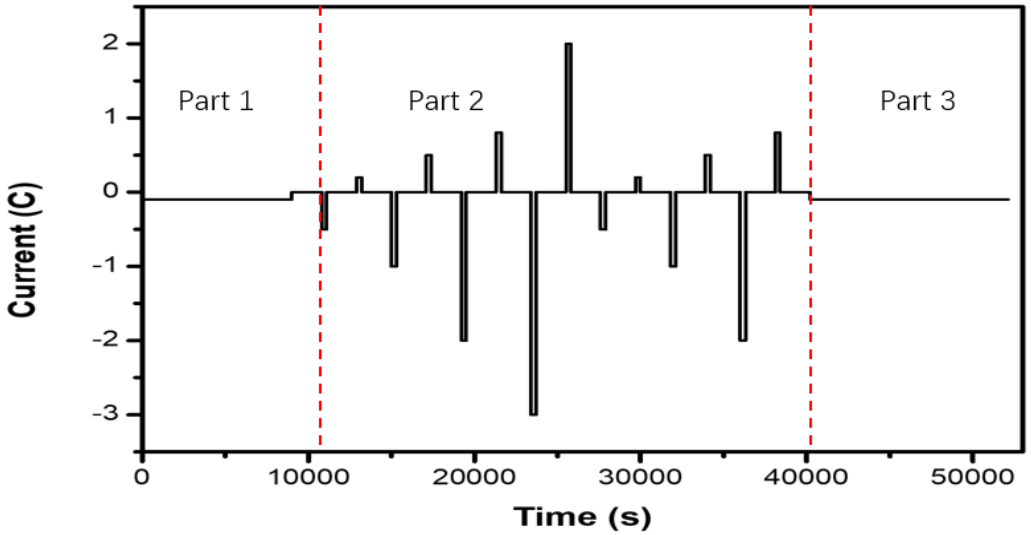

Figure 1. Plot of the current versus time under specific operating conditions.

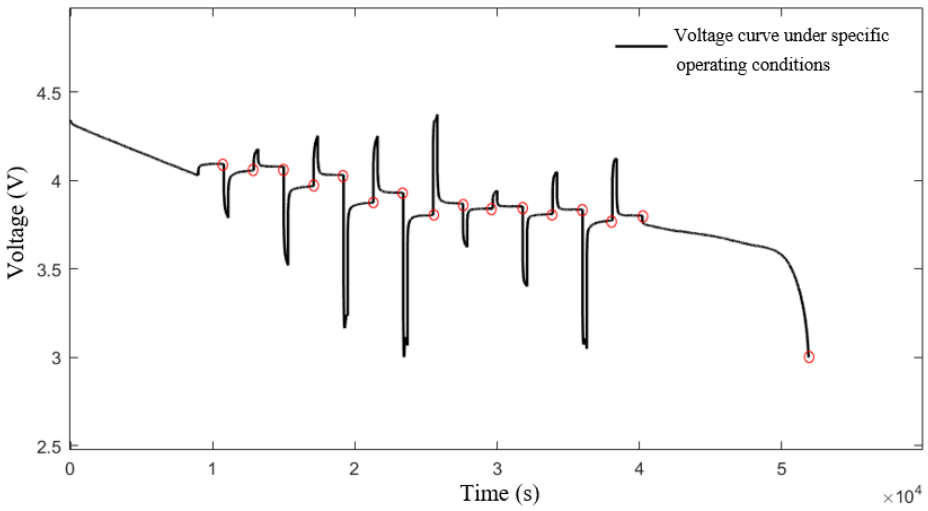

Figure 2. Plot of the voltage response versus time under specific operating conditions.

Fig. 2 shows the voltage response of the battery under specific operating conditions. The model parameters can be determined from the plot by following these steps:

(1) The red circles in Fig. 2 denote the battery voltage after each rest period, which is the open circuit voltage (OCV). These points are on the OCV-SOC curve and can be used to determine y0, x0, Δx and Δy.

(2) The ohmic resistance R_{ohm} can be measured by applying a sinusoidal voltage of 1 kHz to the battery at an SOC of 50%. The ohmic polarization can thus be obtained [23].

(3) At the moment when the voltage changes from 0 to a constant value, i.e., the moment when the rest period ends and charging/charging begins, a voltage change of dU occurs, as plotted in Fig. 3. This change comprises the ohmic overpotential and electrochemical reaction overpotential [24].

Combining this result with step (2), the polarization coefficients of the cathode and anode reactions, P_{actp} and P_{actn}, respectively, can be determined.

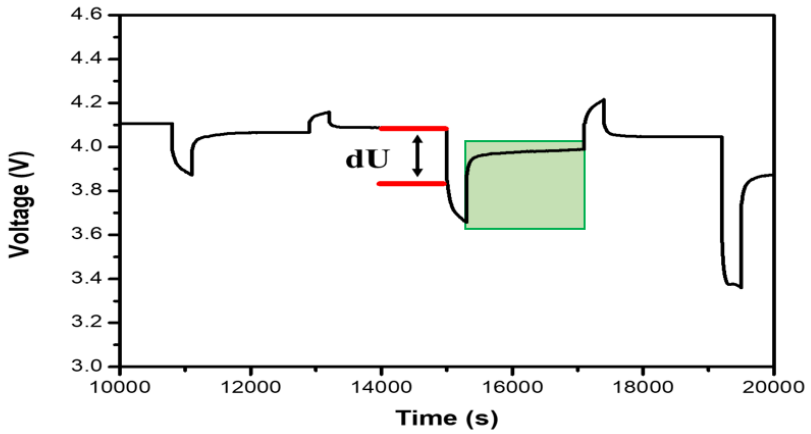

Figure 3. Illustration of the reaction polarization.

a) The green region in Fig. 3 comprises the ohmic overpotential, reaction overpotential, and concentration overpotential [22,24]. By using the ohmic overpotential and the reaction overpotential calculated from steps (2) and (3), the concentration overpotential can be estimated. Thus, the parameters associated with the diffusion process, P_{con}, τ_e, τ_{ps} and τ_{ns}, can be identified.

3. RESULTS AND DISCUSSION

3.1. Model validation and error analysis

A newly formed battery was used for the experimental procedure. The battery has a nominal capacity of 3.3 Ah and an operating voltage window of 3–4.4 V, and the battery parameters are given in Table 3.

Table 3. Battery parameters

Parameters	Units	Values
Loading of cathode active materials	-	97%
Loading of anode active materials	-	97.40%
Cathode thickness/μm	μm	47
Anode thickness/μm	μm	60.5
Cu thickness/μm	μm	6

Al thickness/μm	μm	10
Weight of $LiCoO_2$/g	g	19.399
Cathode density (after formation)/(g/cm^3)	g/cm^3	3.7
Anode density (after formation)/(g/cm^3)	g/cm^3	1.65
Total area of cathode/m^2	m^2	0.115
Total area of anode/m^2	m^2	0.1182

Cycling tests were performed at 7℃ and 25℃ according to the operating protocol illustrated in Fig. 1. The model parameters were determined using the methods demonstrated in Figs. 2 and 3. Tables 4 and 5 provide the results obtained at 7℃ and 25℃, respectively.

Table 4. Parameters used for the battery model at 7℃.

Parameters	Units	Values
x_0	-	0.4582
y_0	-	0.7758
dx	-	0.5029
dy	-	0.7650
Qp	C	20,667
Qn	C	13,586
$\boldsymbol{\tau_e}$	s	372
R_{ohm}	Ω	0.099
$P_{act\,p}$	$\mathbf{m^{-1.5}\,mol^{0.5}\,s}$	100,000
$P_{act\,n}$	$\mathbf{m^{-1.5}\,mol^{0.5}\,s}$	100,000
P_{con}	$\mathbf{mol\,m^{-3}\,A^{-1}}$	114
τ_{ps}	s	321
τ_{ns}	s	92

Table 5. Parameters used for the battery model at 25℃.

Parameters	Units	Values
x_0	-	0.3634
y_0	-	0.9092
dx	-	0.6120
dy	-	0.8914
Qp	C	19,412
Qn	C	13,327
$\boldsymbol{\tau_e}$	s	482
R_{ohm}	Ω	0.059
$P_{act\,p}$	$\mathbf{m^{-1.5}\,mol^{0.5}\,s}$	100,000
$P_{act\,n}$	$\mathbf{m^{-1.5}\,mol^{0.5}\,s}$	120,000
P_{con}	$\mathbf{mol\,m^{-3}A^{-1}}$	77
τ_{ps}	s	283
τ_{ns}	s	72

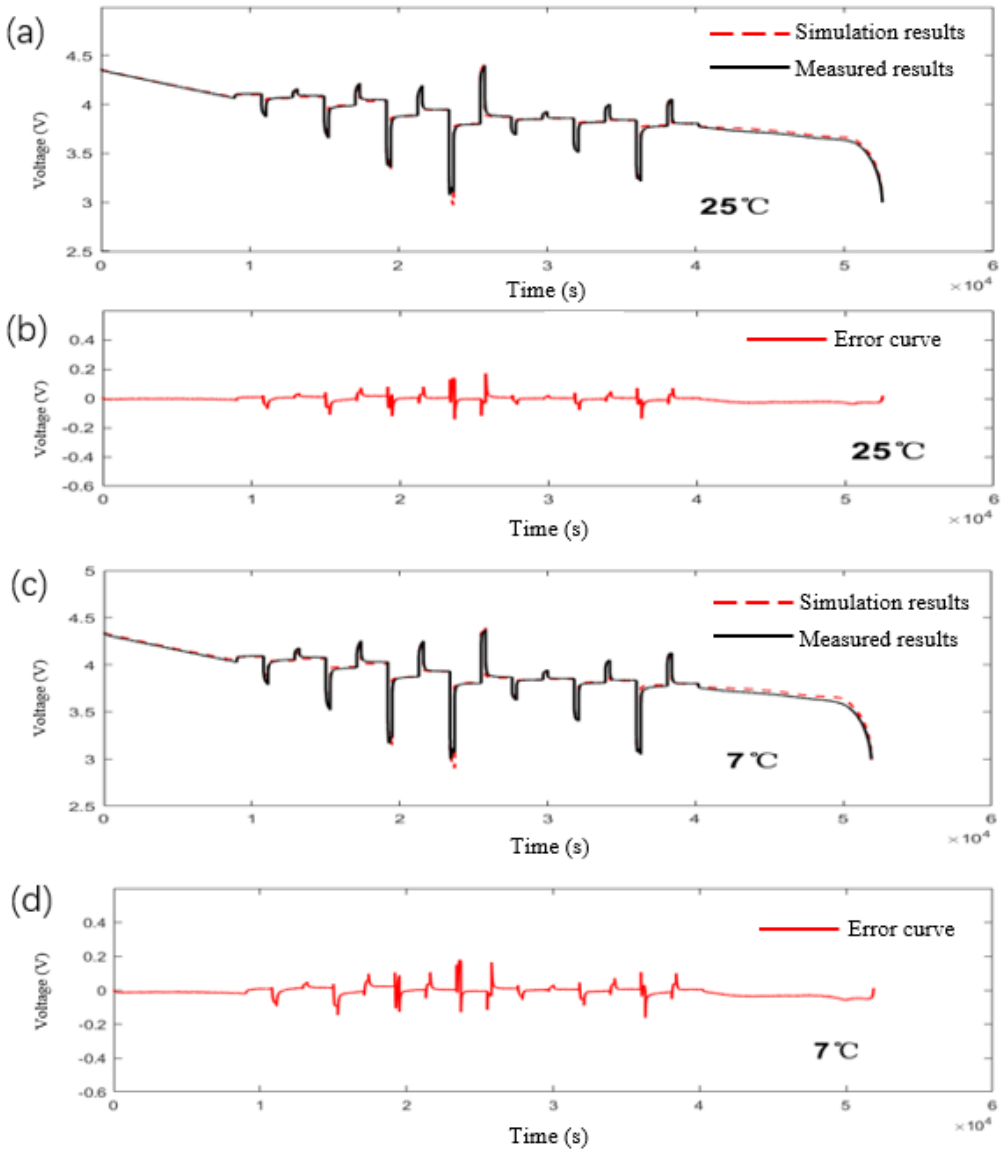

Figure 4. Comparison of the measured and simulated voltages.

Fig. 4(a) compares the measured and simulated voltages of a battery operating under the protocol described in Fig. 1 at 25℃. Fig. 4(b) gives the error curve for the voltage simulation performed at 25℃. The average error of the simulation is 14.2 mV, and the root mean square error is 21.3 mV. Fig. 4(c) compares the measured and simulated voltages of a battery operating under the same protocol at 7℃. Fig. 4(d) shows the error curve obtained for the voltage simulation performed at 7℃. An average error of 20 mV and a root mean square error of 28.4 mV are obtained. Luo and Li et al. identificated the Parameter of SP+ model at 25℃, the average error and the the root-mean-square error between simulated and measured voltages are 19.8 mV and 40.8 mV [21]. The results show that after improving the SP+ model, its accuracy has been improved. Validations of parameter estimation and charge/discharge behaviors indicate that the developed method for the electrochemical model is effective.

3.2. Allowable maximum charging current

The relationship diagrams of the anode potential and current versus the SOC are shown in Fig. 5 (a) and (b). These diagrams are obtained by substituting the determined parameters into the model. Lithium plating is defined to occur when the anode potential drops below 0 V. It is reasonable to suppose that at a certain SOC, the allowable maximum charging current of a battery is the current when the anode potential reaches 0 V. The relationship between the SOC and the allowable maximum charging current can be obtained based on where the voltage-SOC curve intersects the red dashed line (y=0) in the figure at different rates. As shown in Fig. 5 (b) and (d), during battery charging, the allowable maximum charging current generally shows stepped reductions as the SOC increases. This stepwise reduction effect could be attributed to the staged lithium intercalation process occurring in graphite. The allowable maximum charging current also decreases as the temperature decreases, it is consistent with results by Ringbeck et al., meaning that lithium plating takes place more easily at lower temperatures than at high temperatures [25]. At a given SOC, the battery can operate safely and avoid lithium plating if the charging current is lower than its allowable maximum charging current given in the figure.

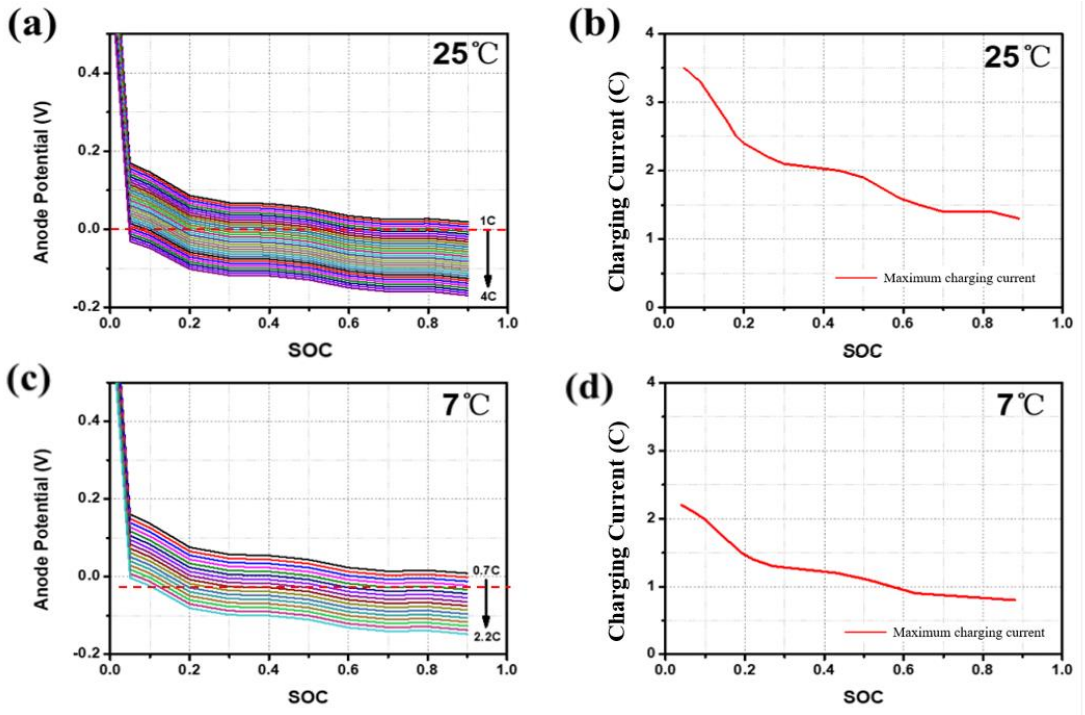

Figure 5. Anode potential and allowable maximum charging current of the battery at different temperatures.

3.3 Result verification

Lithium plating on anodes can be detected in full batteries with reference electrode [26-28]. However, commercial batteries do not contain a reference electrode. Burn et al. describes a charging strategy that charged batteries at different C-rates then opened them to detect lithium plating [29].A

similar approach was used by Zhang, who investigated a stepwise charging strategy to avoid lithium plating [30].

Based on above method, we show a method of cyclic step charging and discharging to verify the safety boundary of lithium-ion battery. The experimental steps are as follows:

(1) Four unused new batteries are activated and numbered No. 1, No. 2, No. 3, and No. 4.

(2) The No. 1 and No. 2 batteries are placed in a thermal chamber at 7 ℃, and the No. 3 and No. 4 batteries are placed in another thermal chamber at 25 ℃ for the cyclic step charging and discharging experiment. Fig. 6 (a) to (d) plots the charging conditions of the No. 1, No. 2, No. 3, and No. 4 batteries, respectively. The discharge condition is a 1 C constant current while discharging to 2.75 V. The number of cycles is 20.

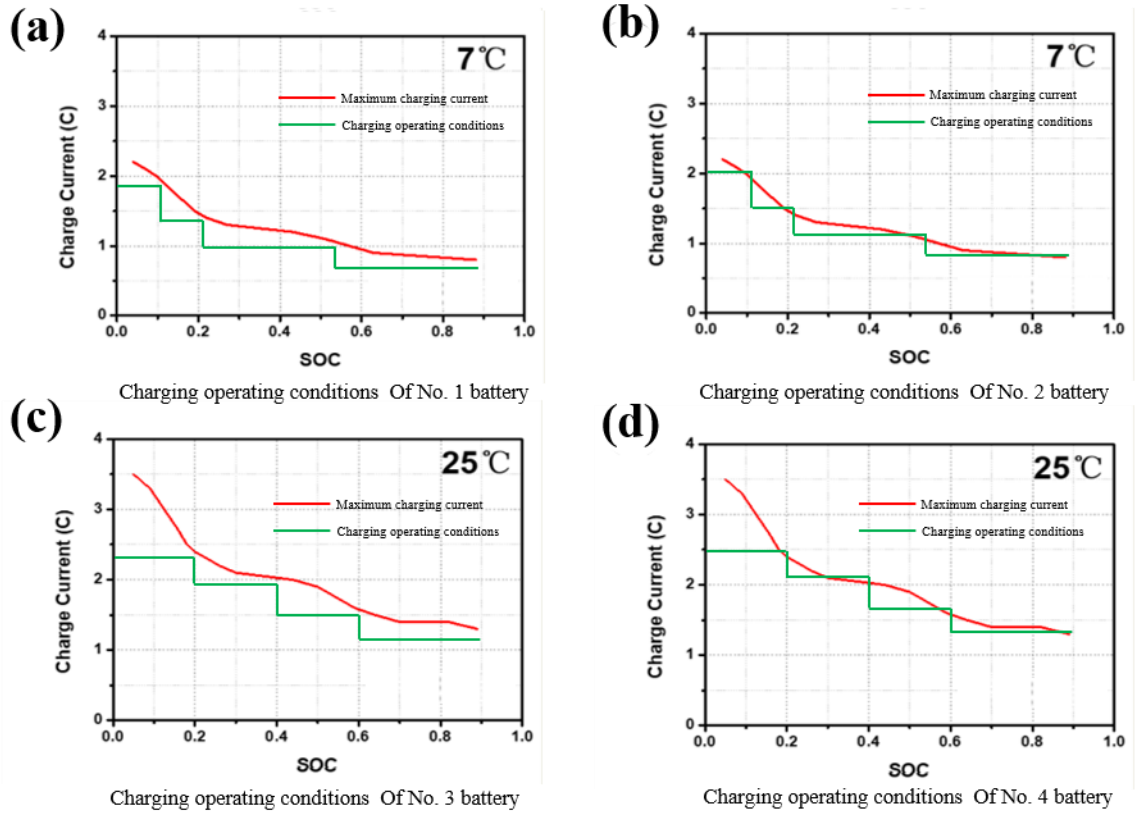

Figure 6. Charging operating conditions used for the verification experiment

After the experiment, the battery is charged at 0.1 C to reach 4.2 V with a constant current and voltage, and the cut-off current is 0.02 C.

Observe the negative electrode surface after disassembling the battery. A photograph of the negative electrode surface is shown in Fig. 7 (a) to (d). Observations show that there are no impurities on the anode surface of the No. 1 and No. 3 batteries, and no lithium plating occurs; there is a gray white material on the anode surface of the No. 2 and No. 4 batteries, and lithium plating occurred. Thus, the maximum charging current curve obtained in this paper has a high prediction accuracy.

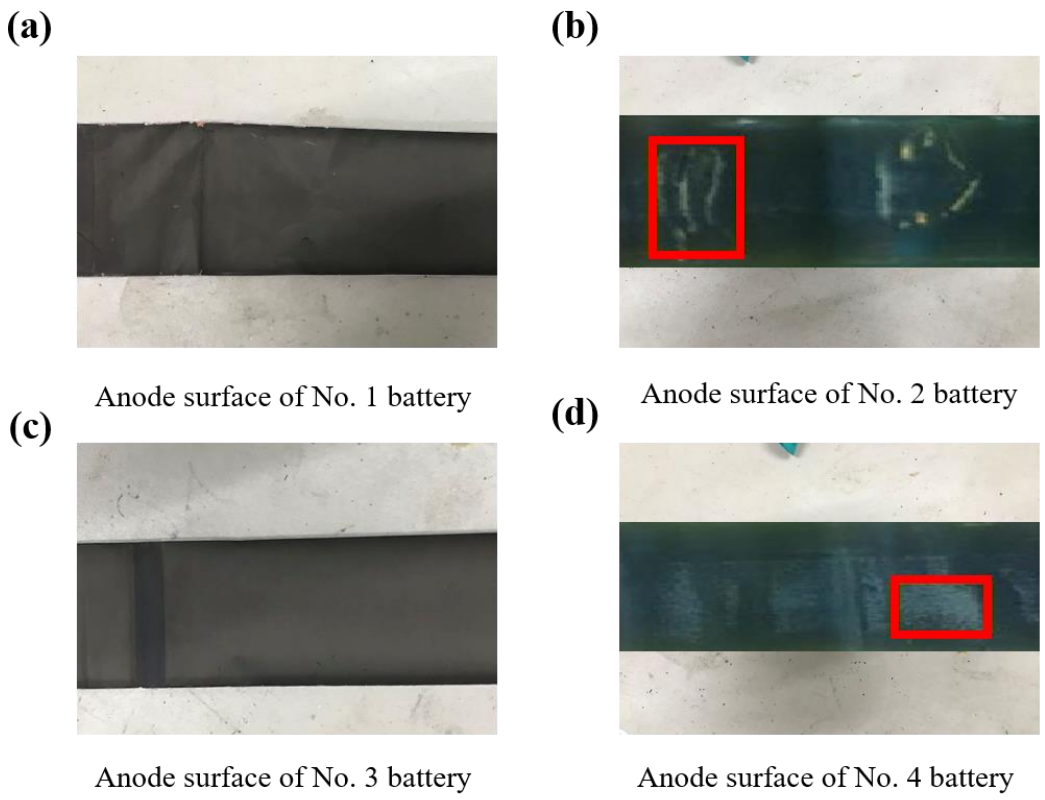

Figure 7. Photographs of the anode surfaces

4. CONCLUSIONS

This paper identifies the relationship between the allowable maximum charging current and the SOC of Li-ion batteries through electrochemical modeling and parameter identification. Lithium plating was used as the threshold in simulations. This method has the following advantages:

(1) The parameters used in the electrochemical model are divided into cathode parameters and anode parameters, which enables this model to accurately simulate the anode potential of Li-ion batteries.

(2) The developed electrochemical model is relatively simple and contains few parameters, and these parameters can be determined under simple operating conditions.

(3) This method provides a relatively high simulation accuracy at different temperatures. At 7°C, the average error is 20 mV, and the root mean square error is 28.4 mV; at 25°C, the average error is 14.2 mV, and the root mean square error is 21.3 mV.

ACKNOWLEDGMENTS
This work was supported by the Key-Area Research and Development Program of Guangdong Province, China (2019B090910002, 2020B090921003) and the Science and Technology Program of Guangzhou, China (201802010072).

References

1. J. M. Tarascon and M. Armand, *Nature*, 414(2001) 359.
2. R. Liu, J. Chen, J. Xun, K. Jiao and Q. Du, *Appl. Energy*, 132(2014) 288.
3. J. Yang, Z. Peng, Z. Pei, Y. Guan, H. Yuan and L. Wu, *Int. J. Electrochem. Sci.*, 13(2018) 9257.
4. Y. Bao, Y. Fan, Y. Chu, C. Ling, X. Tan and S. Yang, *J. Energy Eng.*, 145(2019).
5. Y. Fan, Y. Bao, C. Ling, Y. Chu, X. Tan and S. Yang, *Appl Therm Eng.*, 155(2019) 96.
6. C. Yuan, B. Wang, H. Zhang, C. Long and H. Li, *Int. J. Electrochem. Sci*., 13(2018) 1131.
7. W. Mu, X. Liu, Z. Wen and L. Liu, *J. Energy Storage*, 26(2019) 100921.
8. R. Akolkar, *J. Power Sources*, 232(2013) 23.
9. X. Hu, S. Li and H. Peng, *J. Power Sources*, 198(2012) 359.
10. X. Hu, F. Sun and Y. Zou, *Simul. Modell. Pract. Theory*, 34(2013) 1.
11. M. Dubarry and B. Y. Liaw, *J. Power Sources*, 174(2007) 856.
12. Y. Hu, S. Yurkovich, Y. Guezennec and B. J. Yurkovich, *J. Power Sources*, 196(2011) 449.
13. X. Han, M. Ouyang, L. Lu and J. Li, *J. Power Sources*, 278(2015) 802.
14. N. A. Chaturvedi, R. Klein, J. Christensen, J. Ahmed and A. Kojic, *IEEE Control Syst. Mag.*, 30(2010) 49.
15. T. F. Fuller, M. Doyle and J. Newman, *J. Electrochem. Soc.*, 141(1994) 1.
16. T. F. Fuller, M. Doyle and J. Newman, *J. Electrochem. Soc.*, 141(1994) 982.
17. M. Doyle, T. F. Fuller and J. Newman, *J. Electrochem. Soc*., 140(1993) 1526.
18. J. Vazquez-Arenas, L. E. Gimenez, M. Fowler, T. Han and S.-k. Chen, *Energy Convers. Manage*, 87(2014) 472.
19. S. K. Rahimian, S. Rayman and R. E. White, *J. Power Sources*, 196(2011) 8450.
20. S. K. Rahimian, S. Rayman and R. E. White, *J. Power Sources*, 196(2011) 10297.
21. W. Luo, C. Lyu, L. Wang and L. Zhang, *Microelectron. Reliab.*, 53(2013) 797.
22. J. Li, L. Wang, C. Lyu, E. Liu, Y. Xing and M. Pecht, *Electrochim. Acta*, 275(2018) 50.
23. C. Lyu, Y. Song, J. Zheng, W. Luo, G. Hinds, J. Li and L. Wang, *Appl. Energy*, 250(2019) 685.
24. C. Lyu, Q. Lai, T. Ge, H. Yu, L. Wang and N. Ma, *Energy*, 120(2017) 975.
25. F. Ringbeck, C. Rahe, G. Fuchs and D. U. Sauer, *J. Electrochem. Soc*., 167(2020).
26. H.-P. Lin, D. Chua, M. Salomon, H.-C. Shiao, M. Hendrickson and E. Plichta, *Electrochem. Solid-State Lett*, 4(2011) 71.
27. S.S. Zhang, K. Xu and T.R. Jow, *J. Power Sources*, 160(2006) 1349.
28. T.Waldmann, M. Wilka, M.Kasper, M. Fleischhammer and M. Wohlfahrt-Mehrens, *J. Power Sources*, 262(2014) 219.
29. J. C. Burns, D. A. Stevens and J. R. Dahn, *J. Electrochem. Soc.*, 162(2015) A959.
30. S.S. Zhang, *J. Power Sources* 161(2006) 1385.